Published in final edited form as:
Neuroscience. 2012 September 27; 221: 170–181. doi:10.1016/j.neuroscience.2012.06.052.

SYNAPTIC NMDA RECEPTOR-MEDIATED CURRENTS IN ANTERIOR PIRIFORM CORTEX ARE REDUCED IN THE ADULT FRAGILE X MOUSE

James GOCEL and **John LARSON**
Psychiatric Institute, Department of Psychiatry, College of Medicine, University of Illinois, Chicago, IL 60612

Abstract

Fragile X syndrome is a neurodevelopmental condition caused by the transcriptional silencing of the fragile X mental retardation 1 (*FMR1*) gene. The *Fmr1*-KO mouse exhibits age-dependent deficits in long term potentiation (LTP) at association (ASSN) synapses in anterior piriform cortex (APC). To investigate the mechanisms for this, whole-cell voltage-clamp recordings of ASSN stimulation-evoked synaptic currents were made in APC of slices from adult *Fmr1*-KO and WT mice, using the competitive NMDA receptor antagonist, CPP, to distinguish currents mediated by NMDA and AMPA receptors. NMDA/AMPA current ratios were lower in *Fmr1*-KO mice than in WT mice, at ages ranging from three to 18 months. Since amplitude and frequency of miniature excitatory postsynaptic currents (mEPSCs) mediated by AMPA receptors were no different in *Fmr1*-KO and WT mice at these ages, the results suggest that NMDA receptor-mediated currents are selectively reduced in *Fmr1*-KO mice. Analyses of voltage-dependence and decay kinetics of NMDA receptor-mediated currents did not reveal differences between *Fmr1*-KO and WT mice, suggesting that reduced NMDA currents in *Fmr1*-KO mice are due to fewer synaptic receptors rather than differences in receptor subunit composition. Reduced NMDA receptor signaling may help to explain the LTP deficit seen at APC ASSN synapses in *Fmr1*-KO mice at 6–18 months of age, but does not explain normal LTP at these synapses in mice 3–6 months old. Evoked currents and mEPSCs were also examined in senescent *Fmr1*-KO and WT mice at 24–28 months of age. NMDA/AMPA ratios were similar in senescent WT and *Fmr1*-KO mice, due to a decrease in the ratio in the WT mice, without significant change in AMPA receptor-mediated mEPSCs.

Keywords

Fmr1; FMRP; olfactory cortex; glutamate; long-term potentiation

Corresponding author: Dr. John Larson, Psychiatric Institute (M/C 912), University of Illinois at Chicago, 1601 W. Taylor St., Chicago, IL 60612; Phone: (312) 413-4572; FAX: (312) 413-4569; jrlarson@uic.edu.

Author Contributions: JG and JL designed research; JG performed the experiments; JG and JL analyzed the data and wrote the paper.

DISCLOSURE
The authors declare no conflicts of interest.

INTRODUCTION

Fragile X syndrome (FXS) is the leading cause of inherited intellectual disability and accounts for nearly 5% of autism spectrum disorders (Kelleher and Bear, 2008). In addition to cognitive impairment, FXS is often accompanied by other neuropsychiatric symptoms, including hyperactivity, attention deficits, and seizure disorders. FXS typically results from a trinucleotide expansion in the 5′ UTR of the *FMR1* gene, leading to hyper-methylation and transcriptional silencing (Jin and Warren, 2000). *FMR1* encodes the fragile X mental retardation protein (FMRP), an RNA-binding protein that is highly expressed in brain neurons and associates with a variety of mRNA species to regulate their translation.

Neurobiological studies using mouse models of FXS (*Fmr1*-KO mice) have focused on synaptic function, development, and plasticity, since synaptic communication is critical for the cognitive functions affected in the human disorder. Postmortem studies show immature dendritic spines in FXS cerebral cortex, as seen in mental retardation syndromes generally; these spine abnormalities are also observed in cortex of *Fmr1*-KO mice (Rudelli et al., 1985, Wisniewski et al., 1991, Comery et al., 1997, Irwin et al., 2000). These findings suggest that normal spine development or plasticity depends on FMRP. Many studies have now identified synaptic plasticity deficits involving both LTP (Li et al., 2002, Larson et al., 2005, Zhao et al., 2005, Lauterborn et al., 2007, Wilson and Cox, 2007) and LTD (Huber et al., 2002, Hou et al., 2006) in hippocampus and other cortical regions in *Fmr1*-KO mice. However, the molecular mechanisms responsible for these deficits are not well understood.

Olfactory cortex is an attractive model system for investigating the synaptic basis for behavioral and cognitive dysfunction. Olfactory discrimination learning is impaired by lesions of primary olfactory (piriform) cortex (Staubli et al., 1987) and olfactory training induces synaptic plasticity in piriform cortex (Saar et al., 2002). In *Fmr1*-KO mice, olfactory discrimination learning is impaired, although detection thresholds for odors are normal (Larson et al., 2008). Synapses in anterior piriform cortex (APC) in *Fmr1*-KO mice show an age-dependent impairment of LTP: potentiation at associational (ASSN) system synapses is normal in mice aged 3–6 months, but progressively declines in *Fmr1*-KO mice 6–18 months old (Larson et al., 2005).

LTP in APC depends on activation of NMDA receptors for induction and modification/insertion of AMPA receptors for long-term expression. The present study was undertaken to investigate the possibility that LTP deficits at ASSN synapses in APC of *Fmr1*-KO mice are due to functional changes in synaptic AMPA or NMDA receptors. FMRP binds to ribonucleoprotein complexes in a phosphorylation-dependent manner and influences constitutive and activity-dependent protein translation (Ceman et al., 2003, Narayanan et al., 2008, Darnell et al., 2011). Although FMRP is not known to regulate the translation of ionotropic glutamate receptor mRNAs, it may participate in receptor localization by regulating translation of receptor-binding proteins such as PSD-95 (Muddashetty et al., 2007). We find that NMDA receptor currents are smaller in APC associational synapses of *Fmr1*-KO mice than in those of WT mice, without detectable alterations in their kinetic properties. These results suggest a mechanism that may contribute to both LTP impairment in piriform cortex and defective olfactory learning in mice lacking FMRP.

EXPERIMENTAL PROCEDURES

Animals

Fmr1-KO mice were developed by the Dutch-Belgian Fragile X Consortium (Bakker et al., 1994). Experiments were conducted on littermate *Fmr1*-KO and wild-type (WT) mice bred in the laboratory from congenic C57BL/6J stock obtained from Jackson Laboratories (Bar

Harbor, ME). The mutation had been back-crossed at least ten generations into the C57BL/6 background. Experimental mice (both mutant and control) were obtained from heterozygous *Fmr1*-KO dams mated with either WT or hemizygous *Fmr1*-KO sires. Mice were genotyped by PCR of DNA from ear snips as described previously (Bakker et al., 1994). Experiments and analyses were both conducted blind with respect to genotype. All procedures were in accordance with NIH guidelines and protocols were approved by the Animal Care Committee of the University of Illinois at Chicago.

In vitro slice preparation and electrophysiology

Parasagittal slices (300 μm) of anterior piriform cortex were prepared from adult (3–28 month old) WT and *Fmr1*-KO mice. Mice were decapitated and brains removed in oxygenated artificial CSF (aCSF) containing (in mM): NaCl (120), KCl (3.1), K_2HPO_4 (1.25), $NaHCO_3$ (26), dextrose (5.0), L-ascorbate (2), $MgCl_2$ (1.0), $CaCl_2$ (2.0) at ~4°C. The brain was then sectioned into blocks, mounted on a cutting stage and sliced on a vibrating cutter (Vibratome, St. Louis, MO). The slices were incubated at 32°C for 1 hr and then allowed to cool to room temperature (~25–27°C). Slices were then transferred to a submerged recording chamber and perfused at a rate of 1 ml/min. with aCSF. All drugs and chemicals were applied via the perfusate by a solenoid-controlled gravity-feed system (ValveLink 8, AutoMate Scientific, Inc., Berkeley, CA). Recordings were obtained from principal cells in layer II at room temperature. Patch electrodes (1.8–3 MΩ) contained (in mM): cesium methanesulfonate (145), $MgCl_2$ (1), HEPES (10), BAPTA (1.1), MgATP (5), and phosphocreatine (20) adjusted to pH 7.2 with CsOH, 290 mOsm. The following drugs were added via the perfusate: 3-[(R)-2-carboxypiperazin-4-yl]-prop-2-enyl-1-phosphonic acid (CPP), 6-cyano-7-nitroquinoxaline-2,3-dione (CNQX), 1(S),9(R)-(−)-bicuculline methiodide (BMI), and tetrodotoxin (TTX) (all obtained from Sigma, St. Louis, MO). Cells were visualized with differential interference contrast (DIC) optics on a Nikon Eclipse E600FN “PhysioStation” (Nikon, Melville, NY). Twisted bipolar electrodes (custom made) with a tip diameter ~100 μm were positioned in layer Ib 150–200 μm away from the recorded neuron. Stimulation in this layer activates recurrent association (ASSN) fibers projecting from principal cells in layer II. Responses at these synapses display paired-pulse depression whereas stimulation of afferent fibers in layer Ia exhibit facilitation (Bower and Haberly, 1986). Therefore, stimulation of ASSN fibers in layer Ib was confirmed after obtaining whole-cell recording by non-facilitating responses to paired-pulse stimulation at a 200 ms inter-pulse interval (IPI). ASSN fibers were stimulated at 20 s intervals during recordings. Constant current stimulation (0.1 ms) was adjusted to between 70 and 1000 μA in order to elicit a 300 pA response. Evoked EPSCs and miniature EPSCs (mEPSCs) were recorded with an Axopatch-1D and pClamp software (Molecular Devices, Sunnyvale, CA), filtered at 1 kHz, digitized at 10 kHz, and stored on the computer hard drive. Input and series resistance were checked every 20 s throughout experiments. Recordings were rejected if series resistance exceeded 15 MΩ or if input resistance changed more than 20%. Series and whole-cell capacitance compensation were not used. No corrections were made for liquid junction potentials.

Histology

After obtaining electrophysiological recordings, some slices were fixed in 4% paraformaldehyde and cryoprotected in 30% sucrose in PBS. These slices were then resectioned at 30 μm, processed, and stained with 0.1% Cresyl violet.

Data Analysis

NMDA currents were calculated by digitally subtracting composite responses from pharmacologically isolated AMPA currents at +40 mV. Decay time constants were obtained from single and double exponential fits of spontaneous and evoked responses using

ClampFit software (Molecular Devices). Evoked responses (10 consecutive traces averaged) and mEPSCs (>100 traces averaged) were fit with the standard exponential equation $I(t) = I*\exp(-t/\tau)$, where I is the peak amplitude and τ is a the decay time constant. A weighted time constant (τ_w) was calculated for each trace, except for the mEPSCs, with the equation $\tau_w = [I_F/(I_F + I_S)] * \tau_F + [I_S/(I_F + I_S)] * \tau_S$. The percentage of the decay kinetics mediated by the fast component ($_F$) relative to the slow component (τ_S) was calculated as $\%\tau_F = I_F/(I_F + I_S)$. Current-voltage plots (4 traces averaged) were obtained by ramping membrane potentials sequentially from −80 mV to +40 mV (or from +40 mV to −80 mV) in 10 mV intervals. All data are presented as means ± SEM. Statistical differences were calculated using Student's unpaired *t*-test or the Kolmogorov-Smirnov test if the data were not normally distributed. Analysis of variance was used for comparisons involving more than two groups.

RESULTS

Associational system synaptic currents in APC slices

Voltage clamp recordings in the whole-cell configuration were obtained from layer II cells in slices of anterior piriform cortex (APC) (Fig. 1A). At a holding potential of −80 mV using pipettes filled with a cesium-based internal solution, stimulation of associational (ASSN) system fibers in layer Ib elicited inward currents consisting of an early component mediated by AMPA receptors and a slower component mediated by $GABA_A$ receptors (Fig. 1B). The latter component was routinely blocked by bath perfusion of the $GABA_A$ receptor antagonist, BMI (25 M). ASSN fiber stimulation could be readily distinguished from afferent (lateral olfactory tract; LOT) stimulation by the minimal paired-pulse facilitation or small depression at ASSN fibers in contrast to the robust facilitation of LOT synapses (Fig. 1C) (Bower and Haberly, 1986). In the presence of BMI, ASSN fiber stimulation at high intensity could elicit polysynaptic activity (data not shown); however, at stimulus intensities evoking EPSCs 100–500 pA in amplitude, responses were apparently monosynaptic. For most of the experiments, stimulus intensity was adjusted in order to evoke an EPSC with a peak amplitude of about 300 pA at a holding potential of −80 mV.

Comparison of synaptic currents recorded at holding potentials of −80 mV and +40 mV revealed the coexistence of responses mediated by AMPA and NMDA receptors. At +40 mV, outward currents were considerably prolonged relative to inward currents recorded at −80 mV (Fig. 1D); the slow outward current at +40 mV was blocked by the NMDA antagonist CPP and the fast outward component was blocked by the AMPA receptor antagonist CNQX. Current-voltage relations confirmed that currents isolated by CPP application were relatively linear (Fig. 1E) whereas currents measured in the presence of CNQX (Fig. 2E) demonstrated voltage dependence, hence were mediated by AMPA receptors and NMDA receptors, respectively.

NMDA/AMPA ratio is reduced in the 3–6 month old *Fmr1*-KO mouse

APC layer II cells from *Fmr1*-KO and littermate WT mice were first held at −80 mV in BMI to elicit monosynaptic AMPA-mediated synaptic currents 300–500 pA in peak amplitude. Similar stimulation currents were needed to evoke synaptic currents in slices from WT and KO mice at −80 mV. The holding potential was then ramped to +40 mV in order to obtain composite responses mediated by both AMPA and NMDA receptors. After collecting 10–20 stable responses, CPP (20 μM) was added to the perfusate to block NMDA receptors and a series of traces representing the AMPA receptor-mediated component were obtained. The NMDA receptor-mediated component was constructed by subtracting the average trace recorded in CPP from the average composite response (Fig. 2A). The NMDA/AMPA ratio was calculated for each cell, based on the peak amplitudes of the pharmacologically isolated

responses. The NMDA/AMPA ratio was significantly reduced (34%, $p<.001$) in cells obtained from *Fmr1*-KO mice relative to WT controls (Fig. 2B).

AMPA receptor-mediated mEPSCs are similar in WT and *Fmr1*-KO mice

An alteration in NMDA/AMPA ratio could be due to differences in NMDA receptors, AMPA receptors, or both. In the experiments described above, stimulus intensity was adjusted to evoke similar AMPA receptor responses at −80 mV in both WT and *Fmr1*-KO mice and these components also did not differ at +40 mV (Fig. 2E). With the contribution of AMPA receptors to synaptic currents arbitrarily held constant, NMDA response components were smaller in *Fmr1*-KO mice than in WT mice (Fig. 2D; $p<.05$). In order to obtain independent estimates of AMPA receptor expression at synapses in WT and *Fmr1*-KO mice, miniature EPSCs (mEPSCs) were recorded in the presence of CPP and tetrodotoxin (TTX) to block NMDA receptors and action potential-evoked glutamate release, respectively. BMI was also present to block $GABA_A$ receptors. TTX-resistant mEPSCs are thought to reflect asynchronous, spontaneous release events at individual synapses. The effectiveness of TTX was confirmed by the blockade of evoked EPSCs in response to ASSN fiber stimulation. Spontaneous events were recorded continuously for 400 sec and mEPSCs were identified by a threshold and shape algorithm (Clements and Bekkers, 1997). Application of CNQX abolished the occurrence of these events (data not shown). Recordings from a WT and an *Fmr1*-KO mouse are shown in Fig. 3A and binned amplitude distributions of mEPSCs from the same cells are plotted in Fig. 3B. Data were obtained from 10 WT cells (6 mice) and 17 *Fmr1*-KO cells (7 mice). Amplitude distributions of mEPSCs were skewed in both genotypes; however, they did not differ with respect to mean or median peak amplitude (Fig. 3C and 3D) or mean mEPSC frequency (Fig. 3E). These results suggest that the differences in NMDA/AMPA ratio observed in responses evoked by ASSN fiber stimulation in WT and *Fmr1*-KO mice are not due to differences in AMPA receptor function at individual synapses and are more likely due to decreases in functional synaptic NMDA receptor-mediated currents in the *Fmr1*-KO. However, it must be noted that the mEPSCs recorded in these experiments could also have arisen, in part, from lateral olfactory tract (LOT) synapses as well as ASSN synapses.

Evidence that synaptic AMPA and NMDA receptor kinetics are not altered in *Fmr1*-KO mice

The waveforms of AMPA and NMDA receptor-mediated synaptic currents were also very similar in cells from WT and *Fmr1*-KO mice (Fig. 4). This was true for NMDA receptor-mediated evoked currents obtained by subtraction in CPP at +40 mV (Fig. 4A), evoked AMPA receptor-mediated currents at +40 mV (Fig. 4B) or −80 mV (Fig. 4C), as well as AMPA receptor-mediated mEPSCs at −80 mV (Fig. 4D). The decay phase of mEPSCs were well-fitted by single exponentials and the decay time constants were not significantly different in cells from WT and *Fmr1*-KO mice. AMPA receptor-mediated currents evoked by ASSN fiber stimulation in cells held at −80 mV decayed somewhat more slowly and more variably than mEPSCs: mono-exponential fits did not approximate the evoked current decay phase as well as they did the mEPSCs. Nevertheless, weighted decay time constants based on double exponential fits did not distinguish cells obtained from WT and *Fmr1*-KO mice, either at −80 mV or at +40 mV. Finally, NMDA receptor-mediated evoked currents had similar decay kinetics in cells from *Fmr1*-KO and WT mice; weighted time constants derived from double exponential fits were statistically indistinguishable.

NMDA receptor-mediated synaptic currents have similar voltage sensitivities in *Fmr1*-KO and WT mice

Current-voltage plots for AMPA and NMDA mediated current components were estimated from measurements of ASSN-evoked currents at holding potentials ranging between −80 mV and +40 mV. Recordings were begun at −80 mV or +40 mV and depolarizing or

hyperpolarizing ramps were performed sequentially at 10 mV intervals after four responses were recorded at a given potential. At least 4 traces were averaged at each of a total of 13 holding potentials for each cell included in the analysis (Fig. 5A, B). AMPA and NMDA currents were distinguished by their very different time-course, as described previously (Myme et al., 2003, Harlow et al., 2010, Lo and Zhao, 2011): currents measured at 3 msec after the stimulus are due predominantly to AMPA receptors while currents measured at a 50 msec delay are mediated by NMDA receptors (Fig. 5). The early component (3 msec) showed the linear I/V relation expected for AMPA receptors whereas the late current (50 msec) was non-linear, consistent with Mg^{2+} block of NMDA receptors at negative potentials. Both the early (AMPA) and late (NMDA) components were normalized to their values at +40 mV. Neither the AMPA (Fig. 5C) nor the NMDA (Fig. 5D) components showed significant differences in I/V relations between cells from WT and *Fmr1*-KO mice (repeated measures ANOVA, p>.05).

NMDA/AMPA ratio differences are maintained in mice 6–18 months old

The degree of LTP expressed by APC neurons after theta burst stimulation of ASSN fibers in *Fmr1*-KO mice declines with advancing age (Larson et al., 2005). Synaptic currents from WT and *Fmr1*-KO animals 6–12 and 12–18 months of age were compared in order to determine if alterations to synaptic receptors were the causal mechanism for the increasing deficits to LTP in the aging *Fmr1*-KO mouse. Evoked currents were obtained via the same criteria imposed on experiments performed on the 3–6 month age group. The same general pattern of results observed in mice 3–6 months old were observed in groups of mice aged 6–12 months (Fig. 6) and 12–18 months (Fig. 7). No significant differences were detected in the amount of current used to elicit responses in either genotype in each age group (6–12 mo.; WT 598.16 μA ± 74.47, KO 754.41 μA ± 76.77: $p>0.05$: 12–18 mo.; WT 642.43 μA ± 87.97, KO 437.27 μA ± 119.99: $p>0.05$). Evoked synaptic currents collected from the 6–12 month old animals revealed a reduction (23%) in NMDA/AMPA ratio in the *Fmr1*-KO mice that was similar to that observed in the 3–6 month old *Fmr1*-KO animals, although the difference only approached statistical significance ($p=.08$). The average amplitude of the NMDA component was significantly smaller in the *Fmr1*-KO animals (24%, $p<0.05$) while the AMPA component was equivalent in *Fmr1*-KO and WT mice. Amplitudes and frequencies of AMPA receptor-mediated mEPSCs were identical between genotypes (Fig. 6C). The same trends were observed in the 12–18 month group (Fig. 7). Evoked NMDA/AMPA ratios were significantly lower in *Fmr1*-KO mice compared to WT mice (31%, $p<.05$). AMPA components were similar in mice of both genotypes while NMDA components were reduced in the *Fmr1*-KO (33%, $p=.07$). Frequency and amplitude of AMPA receptor-mediated mEPSCs did not differ for cells from WT and *Fmr1*-KO mice.

Differences in NMDA/AMPA ratios between WT and *Fmr1*-KO mice are not maintained into senescence

Data were also obtained from layer II neurons in APC of a group of littermate WT and *Fmr1*-KO mice at 24 to 28 months of age. Stimulation currents used to obtain composite (AMPA+NMDA) currents at +40 mV were not different in slices from WT and *Fmr1*-KO mice (WT 740.59 μA ± 77.56; KO 654.59 μA ± 88.98, $p>0.05$). In contrast to the earlier ages, NMDA/AMPA ratios were not different between WT and *Fmr1*-KO mice aged 24 months or more (Fig. 8). This appeared to be due to a decrease in NMDA/AMPA ratio in the aged WT mice without a corresponding decrease in NMDA/AMPA ratio in the *Fmr1*-KO mice. Two-way analysis of variance was used to evaluate NMDA/AMPA ratios (peak amplitude) as a function of genotype and age in the entire dataset (Figs. 2, 6, 7, and 8). There were significant main effects of genotype ($\mathbf{F}_{1,142} = 17.61$, $p<.0001$) and age ($\mathbf{F}_{3,142} = 4.69$, $p<.01$) as well as a significant interaction between genotype and age ($\mathbf{F}_{3,142} = 3.08$, $p<.05$). A separate one-way analysis within WT mice showed a significant main effect of age

on the NMDA/AMPA ratio ($\mathbf{F}_{3,72} = 5.91$, $p<.01$), due to a significant decline in the ratio in the 24+ months old group compared to all other ages ($p<.05$, Newman-Keuls tests). A similar one-way analysis within *Fmr1*-KO mice showed no significant effect of age ($\mathbf{F}_{3,70} = 0.70$, $p>.05$).

Evoked NMDA currents had equivalent decay kinetics to young mice (3–6 months of age, WT: 197.42 ms ± 9.90; KO: 181.43 ms ± 13.63, $p>0.05$; 24+ months of age, WT: 181.88 ms ± 12.00; KO: 231.05 ms ± 41.45, $p>0.05$). Analysis of AMPA receptor-mediated mEPSCs did not reveal any significant differences in mEPSC amplitude or frequency between *Fmr1*-KO and WT mice at 24–28 months of age, as at other ages (Fig. 8).

DISCUSSION

There were four principal findings in the present study: (i) the NMDA/AMPA ratio of EPSCs evoked by ASSN fiber stimulation were reduced in APC of adult *Fmr1*-KO mice compared to WT mice, (ii) AMPA receptor mediated mEPSCs in APC neurons were no different in *Fmr1*-KO and WT mice, (iii) Decay kinetics of both AMPA and NMDA receptor-mediated EPSCs were similar in *Fmr1*-KO and WT slices, and (iv) effects of membrane potential on excitatory synaptic currents were unaffected by the presence/absence of FMRP. The former two of these results suggest that NMDA receptor currents are specifically reduced in APC neurons of adult *Fmr1*-KO mice. The latter two findings suggest that the steady-state biophysical properties of the AMPA and NMDA receptors expressed at ASSN synapses are not affected by the lack of expression of FMRP.

NMDA/AMPA ratio of synaptic currents is decreased in APC of adult *Fmr1*-KO mice

We used an electrophysiological approach to measure the relative expression of NMDA- and AMPA- type glutamate receptors at associational (ASSN) synapses on layer II neurons in anterior piriform cortex. Synaptic currents evoked by ASSN fiber stimulation in neurons held under voltage clamp at +40 mV were mediated by both AMPA and NMDA receptors; contributions of the two receptor types to synaptic transmission were resolved using an NMDA receptor antagonist. Comparisons of littermate *Fmr1*-KO and WT mice were made at four different age ranges: 3–6 months, 6–12 months, 12–18 months, and 24–28 months. At each age range (except for the oldest), NMDA/AMPA ratios were lower in *Fmr1*-KO mice than in WT controls. In these experiments, stimulus intensity was set to evoke AMPA receptor-mediated synaptic currents that were similar in peak amplitude in cells from WT and KO mice at −80 mV. Under these conditions, the NMDA-mediated component at +40 mV was smaller in cells from *Fmr1*-KO mice, accounting for the reduced NMDA/AMPA ratio. Although the stimulus intensity is an arbitrary choice, the NMDA/AMPA ratio in voltage-clamped cells should be insensitive to its absolute value.

The present results indicate that the ratio of functional NMDA to AMPA receptor currents at associational synapses in APC is reduced in adult *Fmr1*-KO mice and remains so throughout adulthood until senescence, when the NMDA/AMPA ratio in WT mice declines to the level of *Fmr1*-KO mice. The NMDA/AMPA receptor complement at synapses in adult FMRP-deficient mice may be cell type- or region- specific: medial perforant synapses on granule cells in the hippocampal dentate gyrus exhibit a reduced NMDA/AMPA ratio (Yun and Trommer, 2011), as described here, whereas Schaffer-commissural synapses on CA1 pyramidal neurons show no difference between KO and WT mice (Hu et al., 2008, Pilpel et al., 2009). In the latter case, a greater NMDA/AMPA ratio was observed for synapses in *Fmr1*-KO mice earlier in development (postnatal age 14) (Pilpel et al., 2009). On the other hand, Desai and colleagues found no difference in NMDA/AMPA ratio at synapses on somatosensory cortex pyramidal neurons in *Fmr1*-KO and WT mice at postnatal days 10–18 (Desai et al., 2006). The NMDA/AMPA ratio at early developmental stages in piriform

cortex, as well as the ratio at adult synapses in other regions of cerebral cortex of *Fmr1*-KO mice, remain to be determined.

Synaptic NMDA receptor currents are reduced in APC of *Fmr1*-KO mice

In the presence of TTX, which blocks sodium channels underlying action potentials, excitatory synaptic activity is thought to be due to spontaneous glutamate release; the resulting miniature EPSCs (mEPSCs) reflect asynchronous transmission events at single synapses. In the presence of an NMDA receptor antagonist, mEPSCs mediated by AMPA receptors were compared in WT and *Fmr1*-KO mice. AMPA receptor-mediated mEPSCs recorded from WT and *Fmr1*-KO mice were indistinguishable in terms of frequency of occurrence, peak amplitude, and waveform (kinetics), suggesting that the AMPA receptor composition of synapses on APC neurons is not altered in the absence of FMRP. This suggests that the reduced NMDA/AMPA ratio in *Fmr1*-KO mice reflects a down-regulation of NMDA receptors. We did not directly measure mEPSCs mediated by NMDA receptors since these currents are difficult to resolve due to their prolonged kinetics (Myme et al., 2003), unlike AMPA receptor-mediated mEPSCs, which exhibit fast decay kinetics and can be readily distinguished from one another.

Since the kinetic properties and voltage-dependent gating of NMDA receptor-mediated evoked currents were not detectably different between synapses in WT and *Fmr1*-KO mice, it is unlikely that the reduced NMDA/AMPA ratio in the *Fmr1*-KO is due to compositional changes in NMDA receptors rather than to changes in receptor numbers. For example, retention of spines containing developmentally immature NMDA receptors with a dominant composition of GluN2B rather than GluN2A subunits would be expected to have significantly longer decay kinetics (Vicini et al., 1998). By exclusion, we conclude that the decrease in NMDA/AMPA ratio of evoked synaptic currents in APC of adult *Fmr1*-KO mice is due to fewer functional NMDA receptors at individual synapses. The present results are not consistent with the hypothesis that adult *Fmr1*-KO mice retain a large population of spines with immature “silent” synapses since such silent synapses contain NMDA receptors but lack AMPA receptors (Isaac et al., 1995).

Mechanisms for reduced synaptic NMDA receptor currents in APC of *Fmr1*-KO mice

A decrease in synaptic NMDA receptor currents, as appears to occur at ASSN synapses in APC of the *Fmr1*-KO, could occur in three main ways: First, absence of FMRP could lead to decreased synthesis of NMDA receptor subunits because of altered transcription or mRNA translation. FMRP is believed to regulate protein synthesis by binding to select mRNAs and altering their stability (Zalfa et al., 2007) and/or suppressing translation (Laggerbauer et al., 2001, Li et al., 2001). Although there is little evidence that FMRP directly regulates the translation of glutamate receptor mRNAs, expression of GluN2A can be suppressed by a complex involving FMRP and microRNA-125b (Edbauer et al., 2010). In this context, it is of interest that both GluN2A and GluN2B protein levels were recently found to be decreased in medial prefrontal and orbitofrontal cortices of 2–4 month-old *Fmr1*-KO mice (Krueger et al., 2011).

Second, *Fmr1*-KO mice could have altered trafficking of receptor subunits to synapses (Bagni and Greenough, 2005). NMDA receptors are localized to both synaptic and extra-synaptic sites, defined by whether or not they can be activated by synaptically-released glutamate. Analysis of protein content by immunoblotting does not generally distinguish between these two sites. Trafficking of NMDA receptors to synapses involves both membrane insertion and synaptic localization. Synaptic NMDA receptors reside in the postsynaptic density (PSD) a structure that constitutes a synaptic micro-environment that influences and is influenced by the shape and cytoskeletal organization of the dendritic

spine. Two proteins that are major constituents of the PSD and interact with NMDA receptors are also targets for translational regulation by FMRP. One of these is PSD-95, a membrane-associated guanylate kinase that binds to PDZ domains on the cytoplasmic tails of GluN2A and GluN2B, presumably to control the location and stability of the receptors within the PSD (Bard et al., 2010). FMRP specifically binds to and regulates the translation of *PSD-95* mRNA (Todd et al., 2003, Muddashetty et al., 2007, Zalfa et al., 2007, Muddashetty et al., 2011). The second is CaMKII (Muddashetty et al., 2007), a kinase that phosphorylates NMDA receptor subunits (Omkumar et al., 1996), although how this influences receptor localization is unclear.

Third, synapses in mice lacking FMRP could have suppressed NMDA receptor currents due to post-translational modifications of the receptors themselves or differences in the synaptic micro-environment of the PSD. Multiple kinases and phosphatases interact with C-terminal tails of synaptic NMDA receptors and associated molecular ensembles (MacDonald et al., 1989, Kelso et al., 1992, Tingley et al., 1993, Wang and Salter, 1994, Salter and Kalia, 2004, Braithwaite et al., 2006, Skeberdis et al., 2006) and phosphorylation state can influence channel gating kinetics (Yu et al., 1997, Lan et al., 2001, Krupp et al., 2002, Jones and Leonard, 2005). The absence of significant differences in decay kinetics of NMDA receptor-mediated currents between WT and *Fmr1*-KO mice does not support this mechanism. However, a reduction in channel conductance without a change in kinetics could explain the present results.

NMDA receptors and synaptic plasticity in APC of *Fmr1*-KO mice

We compared excitatory synaptic function in *Fmr1*-KO and WT littermates at ages ranging from three to 28 months. Synaptic NMDA receptors appear to be reduced in APC of *Fmr1*-KO mice throughout adulthood since the NMDA/AMPA ratio was stable in *Fmr1*-KO mice up to 28 months of age; convergence of NMDA/AMPA ratios in senescent mice (24–28 months old) seems to be due to a reduction of the ratio in WT mice rather than to changes in *Fmr1*-KO mice. Our previous work on LTP at ASSN synapses in APC of *Fmr1*-KO mice showed normal LTP at 3–6 months of age but impaired LTP at 6–18 months (Larson et al., 2005).

Reduced synaptic expression of NMDA receptors provides an explanation for impaired LTP in *Fmr1*-KO mice at the older age ranges, but does not explain why LTP is not affected in young adult *Fmr1*-KO mice. It appears that other factors can compensate for the NMDA receptor deficiency in young adult *Fmr1*-KO mice to enable apparently normal LTP. Perhaps the use of minimal stimulation conditions could uncover an LTP deficit in young adult mice that is not evident with supra-maximal LTP induction paradigms (Lauterborn et al., 2007). Although some measures of synaptic structure and function appear to become normalized after the developmental period in *Fmr1*-KO mice (Galvez and Greenough, 2005, Pilpel et al., 2009), the results from piriform cortex indicate that synaptic dysfunction can persist throughout life and even become exacerbated with age.

Acknowledgments

We thank Dr. Stephen M. Logan for his invaluable advice at the inception of this investigation.

GRANTS

This research was supported by a grant from the National Institutes of Health (DC005793).

Abbreviations

aCSF	artificial cerebrospinal fluid
AMPA	α-amino-3-hydroxy-5-methyl-4-isoxazole propionic acid
APC	anterior piriform cortex
ASSN	association
BMI	bicuculline methiodide
CNQX	6-cyano-7-nitroquinoxaline-2,3-dione
CPP	3-[(R)-2-carboxypiperazin-4-yl]-prop-2-enyl-1-phosphonic acid
EPSC	excitatory post-synaptic current
Fmr1	fragile X mental retardation 1
FMRP	fragile X mental retardation protein
FXS	fragile X syndrome
IPI	inter-pulse interval
LOT	lateral olfactory tract
LTD	long-term depression
LTP	long-term potentiation
mEPSC	miniature excitatory post-synaptic current
NMDA	N-methyl-D-aspartate
PSD	post-synaptic density
TTX	tetrodotoxin

References

Bagni C, Greenough WT. From mRNP trafficking to spine dysmorphogenesis: the roots of fragile X syndrome. Nat Rev Neurosci. 2005; 6:376–387. [PubMed: 15861180]

Bakker CE, Verheij C, Willemsen R, van der Helm R, Oerlemans F, Vermey M, Bygrave A, Hoogeveen AT, Oostra BA, Reyniers E, De Boulle K, D'Hooge R, Cras P, van Velzen D, Nagels D, Martin JJ, De Deyn PP, Darby JK, Willems PJ. Fmr1 knockout mice: a model to study fragile X mental retardation. Cell. 1994; 78:23–33. [PubMed: 8033209]

Bard L, Sainlos M, Bouchet D, Cousins S, Mikasova L, Breillat C, Stephenson FA, Imperiali B, Choquet D, Groc L. Dynamic and specific interaction between synaptic NR2- NMDA receptor and PDZ proteins. Proc Natl Acad Sci USA. 2010; 107:19561–19566. [PubMed: 20974938]

Bower JM, Haberly LB. Facilitating and nonfacilitating synapses on pyramidal cells: a correlation between physiology and morphology. Proc Natl Acad Sci USA. 1986; 83:1115–1119. [PubMed: 3081890]

Braithwaite SP, Paul S, Nairn AC, Lombroso PJ. Synaptic plasticity: one STEP at a time. Trends Neurosci. 2006; 29:452–458. [PubMed: 16806510]

Ceman S, O'Donnell WT, Reed M, Patton S, Pohl J, Warren ST. Phosphorylation influences the translation state of FMRP-associated polyribosomes. Hum Mol Genet. 2003; 12:3295–3305. [PubMed: 14570712]

Clements JD, Bekkers JM. Detection of spontaneous synaptic events with an optimally scaled template. Biophys J. 1997; 73:220–229. [PubMed: 9199786]

Comery TA, Harris JB, Willems PJ, Oostra BA, Irwin SA, Weiler IJ, Greenough WT. Abnormal dendritic spines in fragile X knockout mice: maturation and pruning deficits. Proc Natl Acad Sci USA. 1997; 94:5401–5404. [PubMed: 9144249]

Darnell JC, Van Driesche SJ, Zhang C, Hung KY, Mele A, Fraser CE, Stone EF, Chen C, Fak JJ, Chi SW, Licatalosi DD, Richter JD, Darnell RB. FMRP stalls ribosomal translocation on mRNAs linked to synaptic function and autism. Cell. 2011; 146:247–261. [PubMed: 21784246]

Desai NS, Casimiro TM, Gruber SM, Vanderklish PW. Early postnatal plasticity in neocortex of Fmr1 knockout mice. J Neurophysiol. 2006; 96:1734–1745. [PubMed: 16823030]

Edbauer D, Neilson JR, Foster KA, Wang CF, Seeburg DP, Batterton MN, Tada T, Dolan BM, Sharp PA, Sheng M. Regulation of synaptic structure and function by FMRP-associated microRNAs miR-125b and miR-132. Neuron. 2010; 65:373–384. [PubMed: 20159450]

Galvez R, Greenough WT. Sequence of abnormal dendritic spine development in primary somatosensory cortex of a mouse model of the fragile X mental retardation syndrome. Am J Med Genet A. 2005; 135:155–160. [PubMed: 15880753]

Harlow EG, Till SM, Russell TA, Wijetunge LS, Kind P, Contractor A. Critical period plasticity is disrupted in the barrel cortex of FMR1 knockout mice. Neuron. 2010; 65:385–398. [PubMed: 20159451]

Hou L, Antion MD, Hu D, Spencer CM, Paylor R, Klann E. Dynamic translational and proteasomal regulation of fragile X mental retardation protein controls mGluR-dependent long-term depression. Neuron. 2006; 51:441–454. [PubMed: 16908410]

Hu H, Qin Y, Bochorishvili G, Zhu Y, van Aelst L, Zhu JJ. Ras signaling mechanisms underlying impaired GluR1-dependent plasticity associated with fragile X syndrome. J Neurosci. 2008; 28:7847–7862. [PubMed: 18667617]

Huber KM, Gallagher SM, Warren ST, Bear MF. Altered synaptic plasticity in a mouse model of fragile X mental retardation. Proc Natl Acad Sci USA. 2002; 99:7746–7750. [PubMed: 12032354]

Irwin SA, Galvez R, Greenough WT. Dendritic spine structural anomalies in fragile-X mental retardation syndrome. Cereb Cortex. 2000; 10:1038–1044. [PubMed: 11007554]

Isaac JT, Nicoll RA, Malenka RC. Evidence for silent synapses: implications for the expression of LTP. Neuron. 1995; 15:427–434. [PubMed: 7646894]

Jin P, Warren ST. Understanding the molecular basis of fragile X syndrome. Hum Mol Genet. 2000; 9:901–908. [PubMed: 10767313]

Jones ML, Leonard JP. PKC site mutations reveal differential modulation by insulin of NMDA receptors containing NR2A or NR2B subunits. J Neurochem. 2005; 92:1431–1438. [PubMed: 15748161]

Kelleher RJ III, Bear MF. The autistic neuron: troubled translation? Cell. 2008; 135:401–406. [PubMed: 18984149]

Kelso SR, Nelson TE, Leonard JP. Protein kinase C-mediated enhancement of NMDA currents by metabotropic glutamate receptors in Xenopus oocytes. J Physiol. 1992; 449:705–718. [PubMed: 1381753]

Krueger DD, Osterweil EK, Chen SP, Tye LD, Bear MF. Cognitive dysfunction and prefrontal synaptic abnormalities in a mouse model of fragile X syndrome. Proc Natl Acad Sci USA. 2011; 108:2587–2592. [PubMed: 21262808]

Krupp JJ, Vissel B, Thomas CG, Heinemann SF, Westbrook GL. Calcineurin acts via the C-terminus of NR2A to modulate desensitization of NMDA receptors. Neuropharmacology. 2002; 42:593–602. [PubMed: 11985816]

Laggerbauer B, Ostareck D, Keidel EM, Ostareck-Lederer A, Fischer U. Evidence that fragile X mental retardation protein is a negative regulator of translation. Hum Mol Genet. 2001; 10:329–338. [PubMed: 11157796]

Lan JY, Skeberdis VA, Jover T, Grooms SY, Lin Y, Araneda RC, Zheng X, Bennett MV, Zukin RS. Protein kinase C modulates NMDA receptor trafficking and gating. Nat Neurosci. 2001; 4:382–390. [PubMed: 11276228]

Larson J, Jessen RE, Kim D, Fine AK, du Hoffmann J. Age-dependent and selective impairment of long-term potentiation in the anterior piriform cortex of mice lacking the fragile X mental retardation protein. J Neurosci. 2005; 25:9460–9469. [PubMed: 16221856]

Larson J, Kim D, Patel RC, Floreani C. Olfactory discrimination learning in mice lacking the fragile X mental retardation protein. Neurobiol Learn Mem. 2008; 90:90–102. [PubMed: 18289890]

Lauterborn JC, Rex CS, Kramar E, Chen LY, Pandyarajan V, Lynch G, Gall CM. Brain-derived neurotrophic factor rescues synaptic plasticity in a mouse model of fragile X syndrome. J Neurosci. 2007; 27:10685–10694. [PubMed: 17913902]

Li J, Pelletier MR, Perez Velazquez JL, Carlen PL. Reduced cortical synaptic plasticity and GluR1 expression associated with fragile X mental retardation protein deficiency. Mol Cell Neurosci. 2002; 19:138–151. [PubMed: 11860268]

Li Z, Zhang Y, Ku L, Wilkinson KD, Warren ST, Feng Y. The fragile X mental retardation protein inhibits translation via interacting with mRNA. Nucleic Acids Res. 2001; 29:2276–2283. [PubMed: 11376146]

Lo FS, Zhao S. N-methyl-D-aspartate receptor subunit composition in the rat trigeminal principal nucleus remains constant during postnatal development and following neonatal denervation. Neuroscience. 2011; 178:240–249. [PubMed: 21256193]

MacDonald JF, Mody I, Salter MW. Regulation of N-methyl-D-aspartate receptors revealed by intracellular dialysis of murine neurones in culture. J Physiol. 1989; 414:17–34. [PubMed: 2558167]

Muddashetty RS, Kelic S, Gross C, Xu M, Bassell GJ. Dysregulated metabotropic glutamate receptor-dependent translation of AMPA receptor and postsynaptic density-95 mRNAs at synapses in a mouse model of fragile X syndrome. J Neurosci. 2007; 27:5338–5348. [PubMed: 17507556]

Muddashetty RS, Nalavadi VC, Gross C, Yao X, Xing L, Laur O, Warren ST, Bassell GJ. Reversible Inhibition of PSD-95 mRNA Translation by miR-125a, FMRP Phosphorylation, and mGluR Signaling. MolCell. 2011; 42:673–688.

Myme CI, Sugino K, Turrigiano GG, Nelson SB. The NMDA-to-AMPA ratio at synapses onto layer 2/3 pyramidal neurons is conserved across prefrontal and visual cortices. J Neurophysiol. 2003; 90:771–779. [PubMed: 12672778]

Narayanan U, Nalavadi V, Nakamoto M, Thomas G, Ceman S, Bassell GJ, Warren ST. S6K1 phosphorylates and regulates fragile X mental retardation protein (FMRP) with the neuronal protein synthesis-dependent mammalian target of rapamycin (mTOR) signaling cascade. J Biol Chem. 2008; 283:18478–18482. [PubMed: 18474609]

Omkumar RV, Kiely MJ, Rosenstein AJ, Min KT, Kennedy MB. Identification of a phosphorylation site for calcium/calmodulindependent protein kinase II in the NR2B subunit of the N-methyl-D-aspartate receptor. J Biol Chem. 1996; 271:31670–31678. [PubMed: 8940188]

Pilpel Y, Kolleker A, Berberich S, Ginger M, Frick A, Mientjes E, Oostra BA, Seeburg PH. Synaptic ionotropic glutamate receptors and plasticity are developmentally altered in the CA1 field of Fmr1 knockout mice. J Physiol. 2009; 587:787–804. [PubMed: 19103683]

Rudelli RD, Brown WT, Wisniewski K, Jenkins EC, Laure-Kamionowska M, Connell F, Wisniewski HM. Adult fragile X syndrome. Clinico-neuropathologic findings. Acta Neuropathol(Berl). 1985; 67:289–295. [PubMed: 4050344]

Saar D, Grossman Y, Barkai E. Learning-induced enhancement of postsynaptic potentials in pyramidal neurons. J Neurophysiol. 2002; 87:2358–2363. [PubMed: 11976373]

Salter MW, Kalia LV. Src kinases: a hub for NMDA receptor regulation. Nat Rev Neurosci. 2004; 5:317–328. [PubMed: 15034556]

Skeberdis VA, Chevaleyre V, Lau CG, Goldberg JH, Pettit DL, Suadicani SO, Lin Y, Bennett MV, Yuste R, Castillo PE, Zukin RS. Protein kinase A regulates calcium permeability of NMDA receptors. Nat Neurosci. 2006; 9:501–510. [PubMed: 16531999]

Staubli U, Schottler F, Nejat-Bina D. Role of dorsomedial thalamic nucleus and piriform cortex in processing olfactory information. Behav Brain Res. 1987; 25:117–129. [PubMed: 3675824]

Tingley WG, Roche KW, Thompson AK, Huganir RL. Regulation of NMDA receptor phosphorylation by alternative splicing of the C-terminal domain. Nature. 1993; 364:70–73. [PubMed: 8316301]

Todd PK, Mack KJ, Malter JS. The fragile X mental retardation protein is required for type-I metabotropic glutamate receptor-dependent translation of PSD-95. Proc Natl Acad Sci USA. 2003; 100:14374–14378. [PubMed: 14614133]

Vicini S, Wang JF, Li JH, Zhu WJ, Wang YH, Luo JH, Wolfe BB, Grayson DR. Functional and pharmacological differences between recombinant N-methyl-D-aspartate receptors. J Neurophysiol. 1998; 79:555–566. [PubMed: 9463421]

Wang YT, Salter MW. Regulation of NMDA receptors by tyrosine kinases and phosphatases. Nature. 1994; 369:233–235. [PubMed: 7514272]

Wilson BM, Cox CL. Absence of metabotropic glutamate receptor-mediated plasticity in the neocortex of fragile X mice. Proc Natl Acad Sci USA. 2007; 104:2454–2459. [PubMed: 17287348]

Wisniewski KE, Segan SM, Miezejeski CM, Sersen EA, Rudelli RD. The Fra(X) syndrome: neurological, electrophysiological, and neuropathological abnormalities. Am J Med Genet. 1991; 38:476–480. [PubMed: 2018089]

Yu XM, Askalan R, Keil GJ, Salter MW. NMDA channel regulation by channel-associated protein tyrosine kinase Src. Science. 1997; 275:674–678. [PubMed: 9005855]

Yun SH, Trommer BL. Fragile X mice: reduced long-term potentiation and N-Methyl-D-Aspartate receptor-mediated neurotransmission in dentate gyrus. J Neurosci Res. 2011; 89:176–182. [PubMed: 21162125]

Zalfa F, Eleuteri B, Dickson KS, Mercaldo V, De Rubeis S, Di Penta A, Tabolacci E, Chiurazzi P, Neri G, Grant SG, Bagni C. A new function for the fragile X mental retardation protein in regulation of PSD-95 mRNA stability. Nat Neurosci. 2007; 10:578–587. [PubMed: 17417632]

Zhao MG, Toyoda H, Ko SW, Ding HK, Wu LJ, Zhuo M. Deficits in trace fear memory and long-term potentiation in a mouse model for fragile X syndrome. J Neurosci. 2005; 25:7385–7392. [PubMed: 16093389]

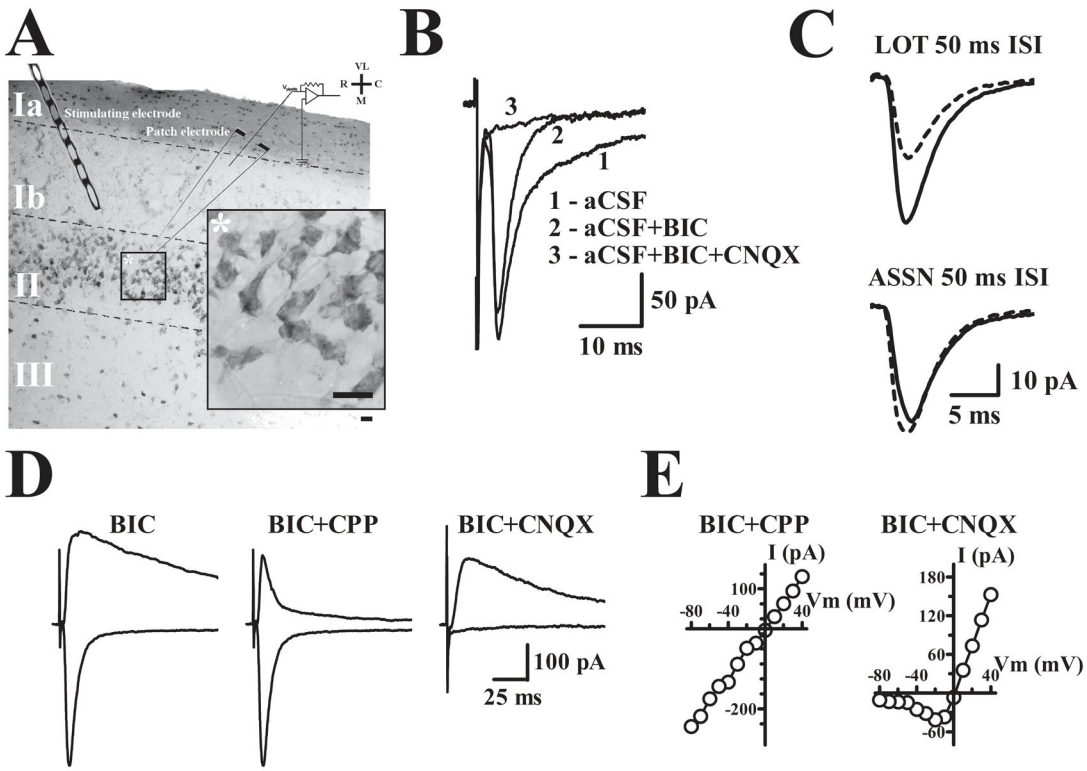

Figure 1. Physiological and anatomical properties of principal cells in APC

A. 30 μm thick APC section stained with Cresyl violet and resectioned from a 300 μm thick 3–6 months old WT slice used in physiological recordings. ASSN synapses were stimulated with an electrode placed in layer Ib. Calibration bar, whole section: 100μm; inset: 10 μm. VL, ventrolateral; R, rostral; C, caudal; M, medial. **B.** Evoked recordings were initially obtained at −80 mV. Bicuculline (BIC) was included in the artificial cerebrospinal fluid (aCSF) perfusate to block inhibitory currents and reveal AMPA receptor mediated currents sensitive to AMPA receptor antagonist CNQX. **C.** Paired-pulse stimulation produces robust facilitation of lateral olfactory tract synapses in layer Ia and a small depression at ASSN synapses in layer Ib. Dashed line traces represent the initial evoked response and solid line traces represent the event elicited by the second pulse presented at an IPI of 50 ms. **D.** Evoked currents at −80 mV and +40 mV illustrate the pronounced voltage-dependent (NMDA) current component at positive potentials. AMPA and NMDA components of evoked currents were isolated by CPP and CNQX respectively. **E.** Current-Voltage plots for cells in which the AMPA (BIC+CPP) or NMDA (BIC+CNQX) currents were isolated using the indicated drugs.

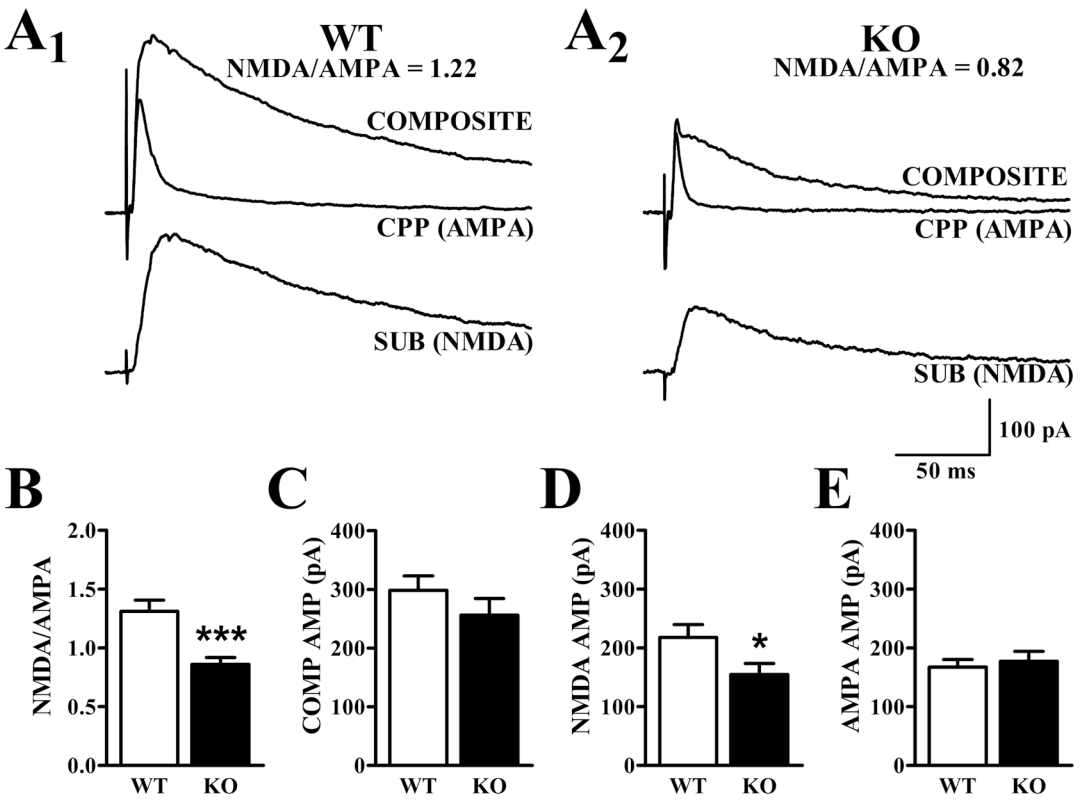

Figure 2. NMDA/AMPA ratio is reduced in APC of *Fmr1*-KO mice

A_1 and A_2. Traces illustrating composite (AMPA + NMDA), pharmacologically-isolated AMPA (in presence of CPP), and inferred NMDA (SUB) currents at +40 mV from representative cells in WT and *Fmr1*-KO mice at 3–6 months of age. **B.** The NMDA/AMPA ratio calculated from the peak amplitude of the NMDA current and that of the AMPA current was significantly lower in cells from *Fmr1*-KO mice than in cells from WT mice (t_{43} = 4.15, p<.001). **C**. Evoked currents with peak amplitudes of 300 pA were obtained at −80 mV before ramping the cell up to +40 mV. Average peak amplitudes of the composite response at positive potentials demonstrated no difference between genotypes (t_{43} = 1.09, p>.2). **D**. The average NMDA current was significantly smaller in *Fmr1*-KO than WT mice (t_{43} = 2.17, p<.05). **E**. Average AMPA currents in *Fmr1*-KO and WT mice at +40 mV were not significantly different (t_{43} = 0.46, p>.6). Data are displayed as mean ± SEM (***: p<.001; *: p<.05).

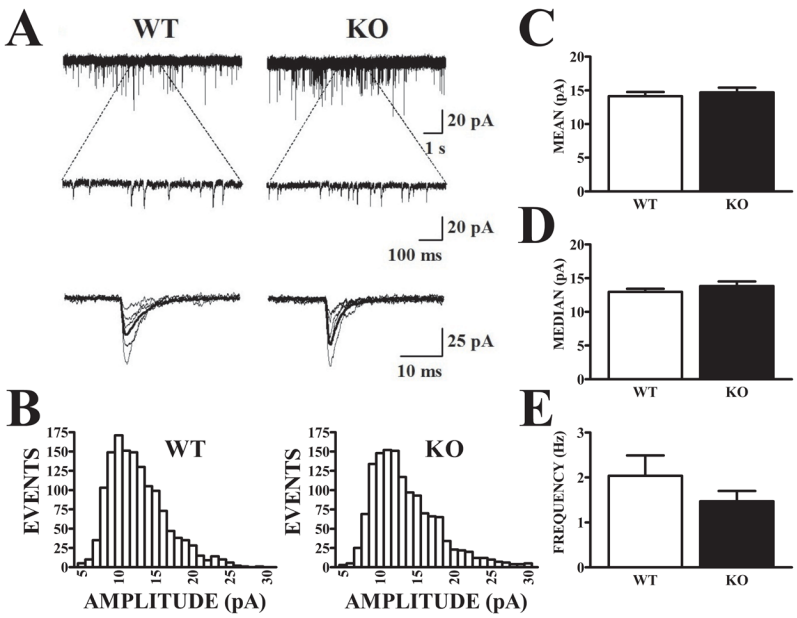

Figure 3. Amplitude and frequency of AMPA receptor-mediated mEPSCs do not differ in APC of *Fmr1*-KO and WT mice

A. AMPA-mediated mEPSCs were recorded in the presence of the NMDA antagonist, CPP, and the sodium channel antagonist, TTX. Recordings show spontaneously-occurring currents from representative WT and *Fmr1*-KO mice at slow (upper) and expanded (lower) sweeps, with captured individual events temporally aligned and superimposed below. **B.** Amplitude histograms of captured events exceeding detection threshold (5 pA) are displayed for the same two cells illustrated in (**A**). Distributions of mEPSCs from the WT and *Fmr1*-KO cells were equally skewed and exhibited no evident differences. Histograms are based on events recorded during a 400 sec period in each cell. **C–D.** Mean mEPSC amplitudes were compared for WT (n = 10) and *Fmr1*-KO (n = 17) cells. Since amplitude histograms were skewed, "average" amplitudes across cells within each group were calculated based on either the mean (**C**) or median (**D**) amplitude for each cell. Neither measure showed a significant difference between genotypes (*t*-tests, $p>.05$) **E.** The average mEPSC frequency observed was also not significantly different ($t_{25} = 1.25$, $p>.2$).

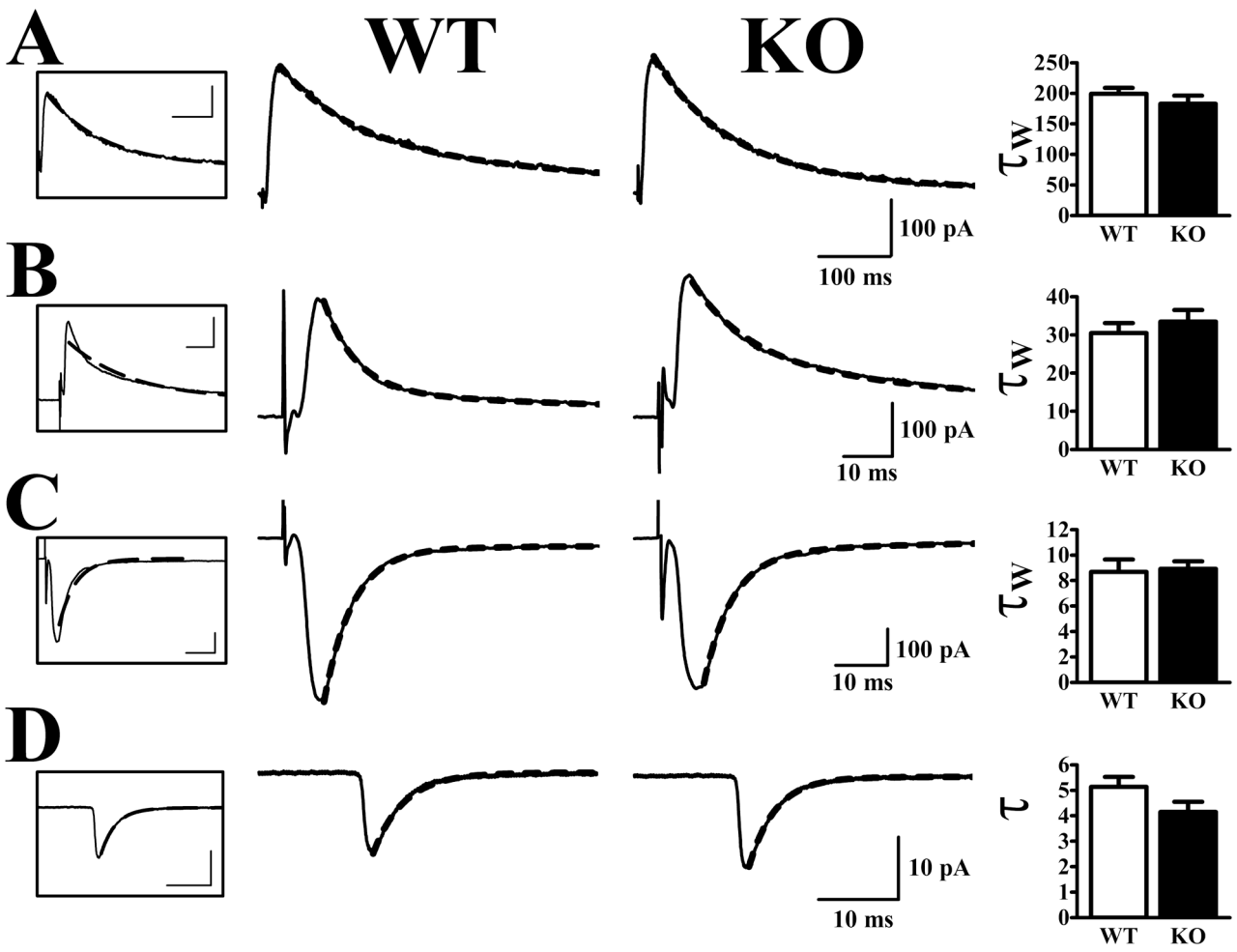

Figure 4. Synaptic current decay kinetics are unaltered in *Fmr1*-KO mice

Traces in middle panels are typical currents recorded from individual cells and are fit with a double-exponential decay functions (dashed lines). Traces boxed on the left are WT currents fit with a single exponent. Bar graphs on the right show averaged decay time constants obtained from cells in each group. **A.** NMDA receptor-mediated currents at +40 mV were well fit by a bi-exponential decay equation (see methods). The weighted time constants ($_W$) did not differ in cells from WT and *Fmr1*-KO mice. **B.** Evoked AMPA currents at +40 mV had longer time constants than at −80 mV (compare with panel **C**) and fit much better with double than with single exponents. The weighted time decay time constants were not different in cells from WT and *Fmr1*-KO mice. **C.** AMPA currents at −80 mV closely reflected the time constant observed in mEPSCs in both genotypes. **D.** AMPA receptor-mediated mEPSCs were well-fit with one exponent and also did not differ in WT and *Fmr1*-KO mice (t_{25} = 1.63, p>.1).

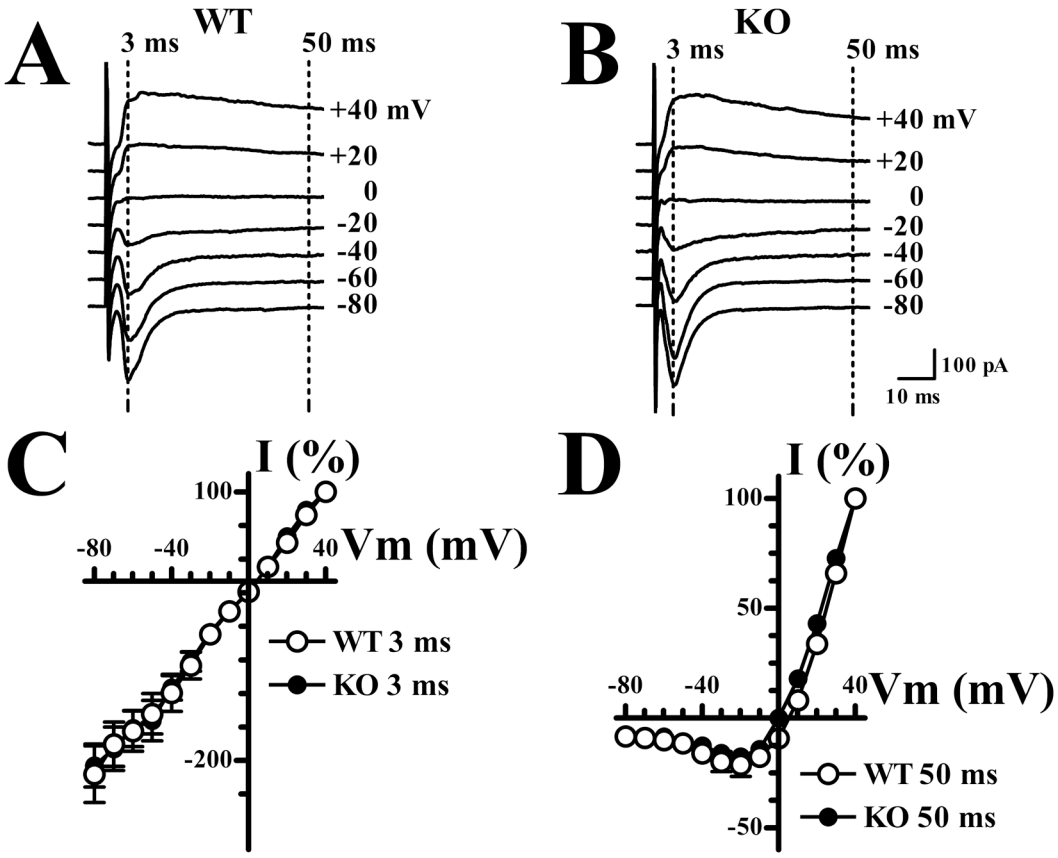

Figure 5. Synaptic NMDA and AMPA receptors show similar current-voltage relations in WT and *Fmr1*-KO mice

A. Currents evoked by ASSN fiber stimulation in a cell from a WT mouse at indicated holding potentials. AMPA receptor mediated components were measured at 3 msec and NMDA receptor-mediated components were measured at 50 msec after the stimulus. **B.** As in **A**, for a cell from a *Fmr1*-KO mouse. **C.** I–V relation for early (AMPA) components in WT (n = 10) and *Fmr1*-KO (n=16) cells. Analysis of variance indicated no significant main effect of genotype ($\mathbf{F}_{1,24} = 0.02$, $p > .05$) or interaction of genotype with holding potential ($\mathbf{F}_{11,264} = 0.12$, $p > .05$). **D.** I–V relation for late (NMDA) components in same cells illustrated in **C**. Analysis of variance indicated no significant main effect of genotype ($\mathbf{F}_{1,24} = 3.25$, $p > .05$) or interaction of genotype with holding potential ($\mathbf{F}_{11,264} = 1.56$, $p > .05$).

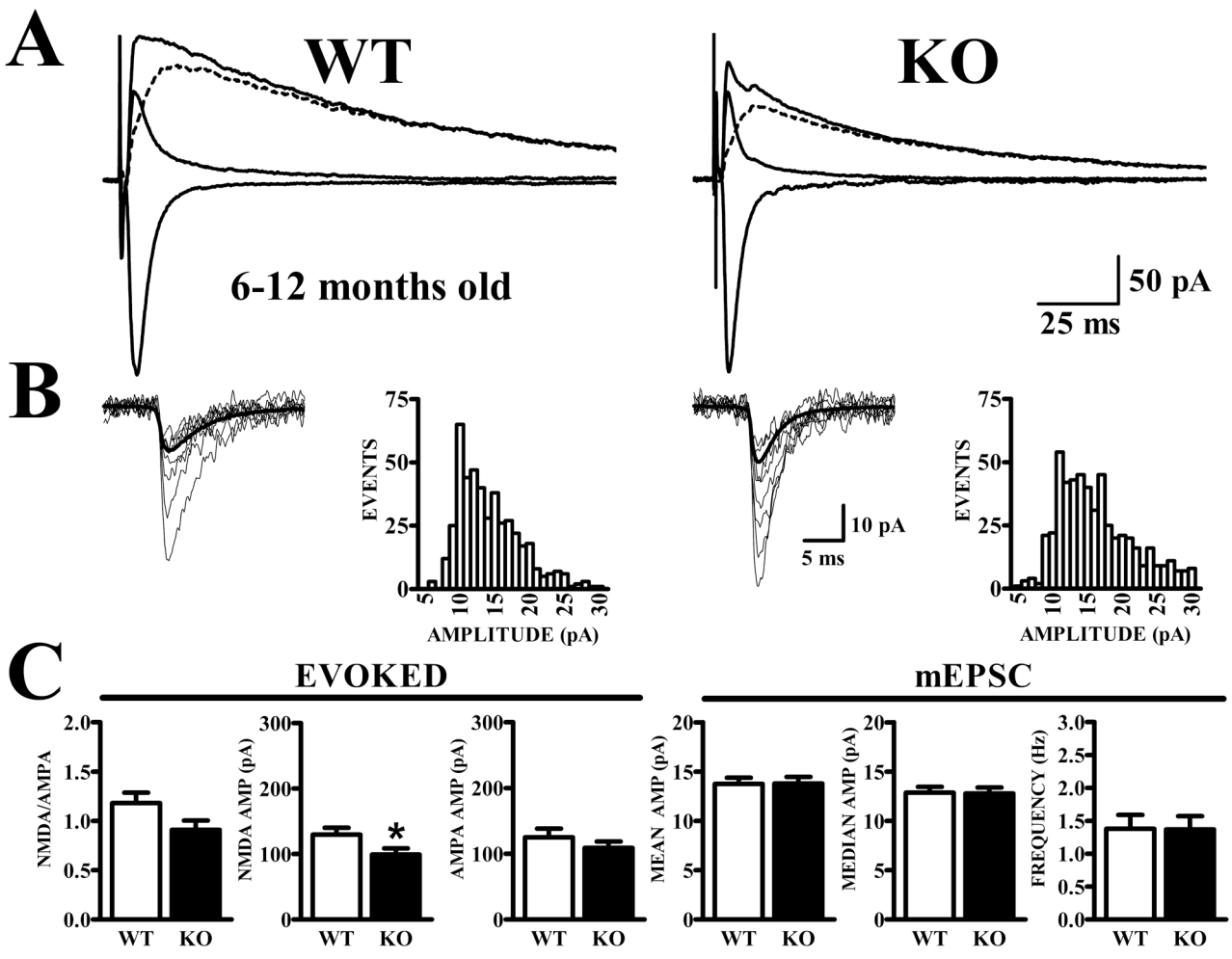

Figure 6. Lower NMDA/AMPA ratio is maintained in *Fmr1*-KO mice at 6–12 months of age

Identical criteria were used to obtain evoked currents from 6–12 month-old WT and *Fmr1*-KO as for 3–6 month-old animals. **A**. Traces show synaptic currents recorded at −80 mV before and at +40 mV before and after CPP, along with the subtracted NMDA current (dashed traces). **B.** mEPSCs exhibit similar amplitude distributions in WT and *Fmr1*-KO mice. **C.** Bar graphs show quantification of NMDA and AMPA currents for evoked synaptic currents (left panels) and mEPSCs (right panels). NMDA/AMPA ratios were not significantly different (t_{37} = 1.83, p=.076); however the average NMDA amplitude was significantly reduced in *Fmr1*-KO mice (t_{37} = 2.24, p<.05). No differences were noted in the average AMPA amplitude comparison (t_{37} = 0.80, p>.4). Measurements of AMPA receptor-mediated mEPSC amplitude (based on either mean or median mEPSC in each cell) and frequency did not distinguish between cells from WT and *Fmr1*-KO mice.

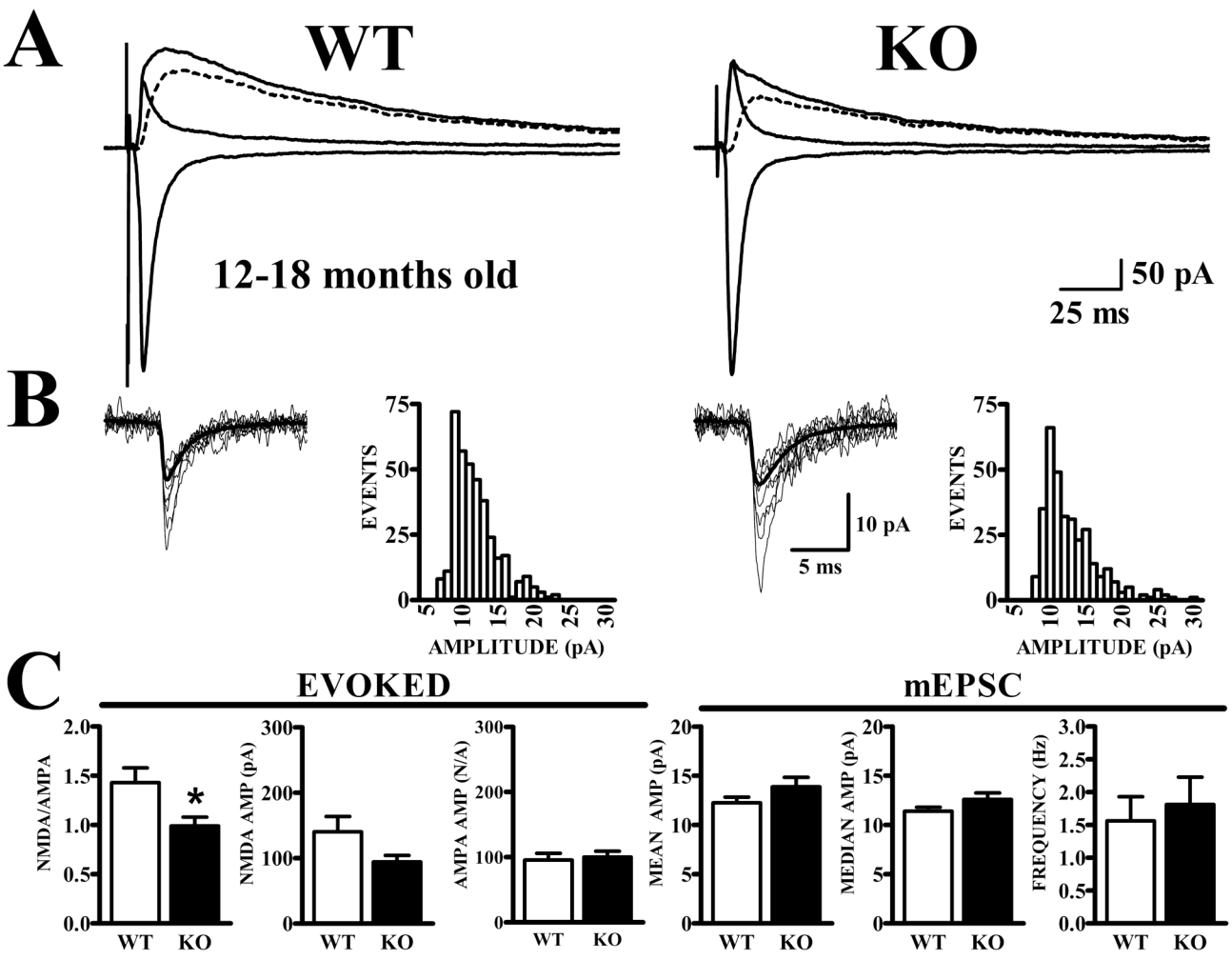

Figure 7. Lower NMDA/AMPA ratio is maintained in *Fmr1*-KO mice at 12–18 months of age

A. Traces show synaptic currents recorded at −80 mV before and at +40 mV before and after CPP, along with the subtracted NMDA current (dashed traces). **B.** mEPSCs exhibit similar amplitude distributions in WT and *Fmr1*-KO mice. **C.** Bar graphs show quantification of NMDA and AMPA currents for evoked synaptic currents (left panels) and mEPSCs (right panels). NMDA/AMPA ratios were significantly lower in cells from *Fmr1*-KO mice (t_{28} = 2.59, p<.05) and the average NMDA current was lower; however this difference did not reach significance (t_{28} = 1.87, p=.072). AMPA currents obtained from WT and *Fmr1*-KO mice were nearly identical. Measurements of AMPA receptor-mediated mEPSC amplitude and frequency did not distinguish between cells from either genotype.

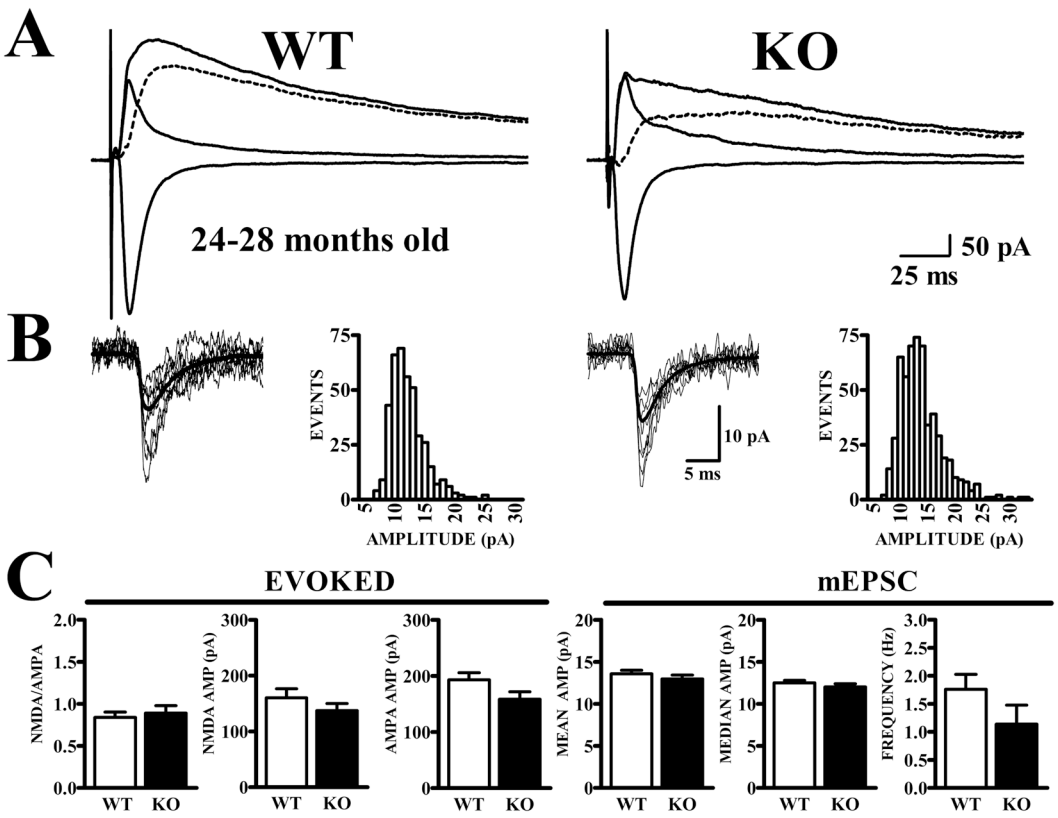

Figure 8. NMDA/AMPA ratios do not differ in APC cells from senescent WT and *Fmr1*-KO mice

Recordings were made from layer II neurons in APC of *Fmr1*-KO and WT mice at 24–28 months of age. **A**. Traces show synaptic currents recorded at −80 mV before and at +40 mV before and after CPP, along with the subtracted NMDA current (dashed traces). **B.** mEPSCs exhibit similar amplitude distributions in WT and *Fmr1*-KO mice. **C.** Bar graphs show quantification of NMDA and AMPA currents and NMDA/AMPA ratios for evoked synaptic currents (left panels) as well as amplitude and frequency of mEPSCs (right panels). Senescent *Fmr1*-KO and WT mice did not differ in NMDA/AMPA ratio (t_{34} = 0.45, p>.6) nor in amplitude of NMDA (t_{34} = 1.29, p>.2) nor amplitude of AMPA (t_{34} = 1.82, p>.05) currents. Measurements of AMPA receptor-mediated mEPSC amplitude and frequency also did not distinguish between cells from WT and *Fmr1*-KO mice.

Excitatory synaptic currents in piriform cortex were compared in Fmr1-KO and WT mice. At 3–18 months of age, NMDA/AMPA ratios were lower in Fmr1-KO than in WT mice. mEPSCs mediated by AMPA receptors were not different in Fmr1-KO and WT mice. At 24–28 months of age, NMDA/AMPA ratios were similar in Fmr1-KO and WT mice.